A triangular virtual element for thin shells

Tiago P. Wu[1], Paulo M. Pimenta[2]

[1]*Dept. of Structural and Geotechnical Engineering, University of São Paulo*
Av. Prof. Almeida Prado, 83, 05508-070, São Paulo, Brazil
tiagowu@usp.br
[2]*Dept. of Structural and Geotechnical Engineering, University of São Paulo*
Av. Prof. Almeida Prado, 83, 05508-070, São Paulo, Brazil
ppimenta@usp.br

Abstract. We propose a low-order triangular element for Kirchhoff-Love shells by the virtual element method, for use in the kinematically linear range. The shell domain discretization by flat triangles enables no use of a predefined mapping approach and curvilinear coordinates system. The displacements and deflection gradient locally defined at the triangle vertices are the local degrees of freedom, corresponding to the lowest-order cases for conforming in-plane and out-of-plane displacement approximations. Accordingly, their respective projections from the finite-dimensional space to linear and quadratic polynomials over the element, supplied by a stabilization, allow defining a (projected) constant strain and curvature virtual element. Numerical examples including stabilization and element geometry extension to quadrilateral for cylindrical shells are used as an illustration of our results.

Keywords: Kirchhoff-Love shell, Linear elasticity, Virtual element method.

1 Introduction

Introduced by Da Veiga et al. [1], the virtual element method (VEM) is a method of arbitrarily polytopal discretization within the Bubnov-Galerkin framework is a generalization of the finite element method. The applications of VEM to the two dimensional elasticity and plate bending originally introduced by Da Veiga et al. [2] and Brezzi and Marini [3], have been explored by, e.g. Mengolini et al. [4] and Wriggers et al. [5], respectively.

This work aims to apply the method for Kirchhoff-Love shells restricted to a flat triangle element geometry and to linearity. By the last, the superposition of effects is allowed. Furthermore, the superposition of membrane and bending behaviors is achieved by the present formulation mostly by unifying aspects of the aforementioned works. The restriction is also made to the method order, the lowest one for conforming approximation of each mentioned behavior. We base on the particular linear case of the shell theory from Pimenta et al. [6] to describe the continuous problem presented in the 2nd section, followed by the methodology applied to discretize it in the 3rd. Our framework is mostly based on the one used in Wriggers et al. [5]. The results are presented in the 4th section by numerical examples including stabilization and element geometry extension to quadrilateral for cylindrical shells.

Unless explicitly indicated, the notations and conventions are Latin and Greek, being regular italic and fraktur lower case letters for scalars (e.g. p, π and $\mathfrak{p}$) and bold for vectors (e.g. $\boldsymbol{p}$, $\boldsymbol{\pi}$ and $\mathfrak{p}$). Bold upright upper case letters are for higher-order tensors (e.g. $\mathbf{P}$ and $\mathbf{\Pi}$) and regular calligraphic or double-struck for sets (e.g. $\mathcal{P}$ and $\mathbb{P}$). In particular, the null vector is $\mathbf{0}$. Regular italic Latin and Greek lower case indices are from $\{1,2,3\}$ and $\{1,2\}$, respectively, with Einstein summation convention except for τ and ν. Only right-handed rectangular systems of axes are used.

2 The continuous problem

Let the shell reference configuration be $V = \Omega \times H$, with middle surface $\Omega \subset \mathbb{R}^2$, sufficiently small constant thickness $h > 0$, $H = (-\frac{h}{2}, \frac{h}{2}) \subset \mathbb{R}$ and mid-surface boundary $\partial\Omega$. With a local orthonormal system $\{\boldsymbol{e}_1^r, \boldsymbol{e}_2^r, \boldsymbol{e}_3^r\}$

on the mid-surface, $\boldsymbol{e}_\alpha^r$ tangent and $\boldsymbol{e}_3^r$ normal to it, the position at reference configuration is

$$\boldsymbol{\xi} = \boldsymbol{\zeta} + \boldsymbol{a}^r = \xi_\alpha \boldsymbol{e}_\alpha^r + \xi_3 \boldsymbol{e}_3^r. \tag{1}$$

The kinematics is here given by the displacement and rotation fields

$$\boldsymbol{u} = \boldsymbol{z} - \boldsymbol{\zeta} \quad \text{and} \quad \boldsymbol{\theta} = -\boldsymbol{e}_3^r \times \nabla u_3, \tag{2}$$

with $\boldsymbol{z}$ the position on the mid-surface at current configuration and $\nabla(\bullet)$ the gradient operator w.r.t. $\boldsymbol{\zeta}$. It leads to the current position

$$\boldsymbol{x} = \boldsymbol{\zeta} + \boldsymbol{u} + \boldsymbol{a}^r + \boldsymbol{\theta} \times \boldsymbol{a}^r = \boldsymbol{z} + \boldsymbol{a}, \tag{3}$$

where the current director may also be given by the linear rotation tensor as $\boldsymbol{a} = \mathbf{Q}\boldsymbol{a}^r = (\mathbf{I} + \text{Skew}(\boldsymbol{\theta}))\boldsymbol{a}^r$, with $\text{Skew}(\bullet)$ as above defined. The deformation of a fiber is given by the deformation gradient

$$\mathbf{F} = \boldsymbol{x}_{,i} \otimes \boldsymbol{e}_i^r = (\boldsymbol{z}_{,\alpha} + \boldsymbol{\theta}_{,\alpha} \times \boldsymbol{a}^r) \otimes \boldsymbol{e}_\alpha^r + \boldsymbol{e}_3 \otimes \boldsymbol{e}_3^r = \mathbf{Q} + (\boldsymbol{\eta}_\alpha + \boldsymbol{\kappa}_\alpha \times \boldsymbol{a}^r) \otimes \boldsymbol{e}_\alpha^r, \tag{4}$$

where we use $\boldsymbol{e}_i = \mathbf{Q}\boldsymbol{e}_i^r$ and the membrane strain and curvature

$$\boldsymbol{\eta}_\alpha = \boldsymbol{z}_{,\alpha} - \boldsymbol{e}_\alpha \quad \text{and} \quad \boldsymbol{\kappa}_\alpha = \boldsymbol{\theta}_{,\alpha}. \tag{5}$$

The linear strain and Cauchy stress tensors for an isotropic linear elastic material are

$$\mathbf{E} = \frac{1}{2}(\mathbf{F} + \mathbf{F}^T - 2\mathbf{I}) \quad \text{and} \quad \mathbf{T} = \lambda \text{tr}(\mathbf{E})\mathbf{I} + 2\mu\mathbf{E}, \tag{6}$$

with $\lambda = \frac{E\nu}{(1-2\nu)(1+\nu)}$ and $\mu = \frac{E}{2(1+\nu)}$ (shear modulus) the Lamé constants, E the Young modulus and ν the Poisson ratio. With the true stresses $\boldsymbol{t}_i$ from $\mathbf{T} = \boldsymbol{t}_i \otimes \boldsymbol{e}_i^r$, acting at planes with normal $\boldsymbol{e}_i^r$, the internal force and moment per unit length are given by the cross-sectional resultants

$$\boldsymbol{n}_\alpha = \int_H \boldsymbol{t}_\alpha \, \mathrm{d}\xi_3 \quad \text{and} \quad \boldsymbol{m}_\alpha = \int_H \boldsymbol{a}^r \times \boldsymbol{t}_\alpha \, \mathrm{d}\xi_3. \tag{7}$$

By the external body force per unit volume $\boldsymbol{f}^b$ and surface traction per unit area $\boldsymbol{f}^t$, the external force and moment per unit area are

$$\bar{\boldsymbol{n}} = \int_H \boldsymbol{f}^b \, \mathrm{d}\xi_3 + \boldsymbol{f}^t \quad \text{and} \quad \bar{\boldsymbol{m}} = \int_H \boldsymbol{a}^r \times \boldsymbol{f}^b \, \mathrm{d}\xi_3 + \boldsymbol{a}^r \times \boldsymbol{f}^t. \tag{8}$$

We gather some of the above quantities as $\boldsymbol{\sigma}_\alpha = [\boldsymbol{n}_\alpha \quad \boldsymbol{m}_\alpha]^T$, $\boldsymbol{\varepsilon}_\alpha = [\boldsymbol{\eta}_\alpha \quad \boldsymbol{\kappa}_\alpha]^T$, $\boldsymbol{q} = [\bar{\boldsymbol{n}} \quad \bar{\boldsymbol{m}}]^T$ and $\boldsymbol{g} = [\boldsymbol{u} \quad \boldsymbol{\theta}]^T$.

From the internal and external powers

$$P_{\text{int}} = \int_V \mathbf{T} : \dot{\mathbf{E}} \, \mathrm{d}\xi = \int_\Omega \boldsymbol{\sigma}_\alpha \cdot \dot{\boldsymbol{\varepsilon}}_\alpha \, \mathrm{d}\zeta \quad \text{and} \quad P_{\text{ext}} = \int_V \boldsymbol{f}^b \cdot \dot{\boldsymbol{x}} \, \mathrm{d}\xi + \int_\Omega \boldsymbol{f}^t \cdot \dot{\boldsymbol{x}} \, \mathrm{d}\zeta = \int_\Omega \boldsymbol{q} \cdot \dot{\boldsymbol{g}} \, \mathrm{d}\zeta, \tag{9}$$

and by the permutability of variation with differentiation and integration processes, the internal virtual work results

$$\begin{aligned} a(\boldsymbol{u}, \boldsymbol{v}) &= \int_\Omega \boldsymbol{\sigma}_\alpha(\boldsymbol{u}) \cdot \boldsymbol{\varepsilon}_\alpha(\boldsymbol{v}) \, \mathrm{d}\zeta \\ &= -\int_\Omega (\nabla \cdot \mathbf{N}(\boldsymbol{u}) \cdot \boldsymbol{v} - \nabla \cdot \nabla \cdot \mathbf{M}(u_3) v_3) \, \mathrm{d}\zeta \\ &\quad + \int_{\partial\Omega} (\mathbf{N}(\boldsymbol{u}) : \boldsymbol{v} \otimes \boldsymbol{\nu} + \mathbf{M}(u_3) : \nabla v_3 \otimes \boldsymbol{\nu} - \nabla \cdot \mathbf{M}(u_3) \cdot \boldsymbol{\nu} v_3) \, \mathrm{d}\tau. \end{aligned} \tag{10}$$

In eq. (10) we use $\boldsymbol{v}$ a virtual displacement, $\mathbf{N} = \boldsymbol{n}_\alpha \otimes \boldsymbol{e}_\alpha^r$, $\mathbf{M} = \boldsymbol{e}_3^r \times \boldsymbol{m}_\alpha \otimes \boldsymbol{e}_\alpha^r$, $\nabla \cdot (\bullet)$ the divergence of $(\bullet)$, $\boldsymbol{\nu}$ the boundary normal and integration by parts twice. The external virtual work is

$$(\boldsymbol{q}, \boldsymbol{g}(\boldsymbol{v})) = \int_\Omega \boldsymbol{q} \cdot \boldsymbol{g}(\boldsymbol{v}) \, \mathrm{d}\zeta = \int_\Omega (\bar{\boldsymbol{n}} \cdot \boldsymbol{v} + \bar{\boldsymbol{m}} \cdot \boldsymbol{\theta}(v_3)) \, \mathrm{d}\zeta. \tag{11}$$

For instance let the boundary to be clamped. The theorem of virtual work or weak form of the problem, with the Sobolev spaces $\mathcal{H}_0^1(\Omega) = \{v \in \mathcal{H}^1(\Omega) : v|_{\partial\Omega} = 0\}$ and $\mathcal{H}_0^2(\Omega) = \{v \in \mathcal{H}^2(\Omega) : v|_{\partial\Omega} = v_{,\nu}|_{\partial\Omega} = 0\}$, results

$$\begin{cases} \boldsymbol{u} \in \boldsymbol{\mathcal{V}}_0 \coloneqq [\mathcal{H}_0^1(\Omega)]^2 \times \mathcal{H}_0^2(\Omega) \\ a(\boldsymbol{u}, \boldsymbol{v}) = (\boldsymbol{q}, \boldsymbol{g}(\boldsymbol{v})), \forall \boldsymbol{v} \in \boldsymbol{\mathcal{V}}_0 \end{cases}. \tag{12}$$

3 Methodology

Unless explicitly indicated, in the sequel we work only with quantities referred to the local system with no correspondent superscript and keep the superscript g for quantities referred to the global system. Superscripts h, α and 3 indicate approximated quantities, in-plane and out-of-plane related quantities, respectively. $N^{(\bullet)}$ stands for "number of $(\bullet)$". The element degrees of freedom (d.o.f.) vector refereed to the global system is $\boldsymbol{d}$.

Let $\{\boldsymbol{e}_1^r, \boldsymbol{e}_2^r, \boldsymbol{e}_3^r\}$ be the canonical basis of $\mathbb{R}^3$ and $\mathbf{R} = \boldsymbol{e}_1^{r,g} \otimes \boldsymbol{e}_1^r + \boldsymbol{e}_2^{r,g} \otimes \boldsymbol{e}_2^r + \boldsymbol{e}_3^{r,g} \otimes \boldsymbol{e}_3^r$ be the local-to-global transformation matrix. Then, $\boldsymbol{v} = \mathbf{R}^T \boldsymbol{v}^g$ for $\boldsymbol{v}^g \in \mathbb{R}^3$. Now, let $\{\boldsymbol{\tau}^g, \boldsymbol{\nu}^g, -\boldsymbol{e}_3^{r,g}\}$ be a local orthonormal system on a polygon edge, with $\boldsymbol{\tau}^g$ the tangent oriented counterclockwise and $\boldsymbol{\nu}^g$ the outward normal. With $\mathbf{R}_{\mathfrak{e}} = \boldsymbol{\tau}^g \otimes \boldsymbol{e}_1^r + \boldsymbol{\nu}^g \otimes \boldsymbol{e}_2^r - \boldsymbol{e}_3^{r,g} \otimes \boldsymbol{e}_3^r$ the correspondent local-to-global transformation matrix, $\boldsymbol{\theta} = \mathbf{R}_{\mathfrak{e}}^T \boldsymbol{\theta}^g$ is the rotation refereed to this local system, from which follows $\nabla v_3^g = \theta_2 \boldsymbol{\tau}^g - \theta_1 \boldsymbol{\nu}^g$ and $\nabla v_3 = \mathbf{R}^T \nabla v_3^g = \theta_2 \boldsymbol{\tau} - \theta_1 \boldsymbol{\nu}$.

Let $\mathfrak{E} \subset \mathbb{R}^2$ be a triangle from a partition $\mathcal{T}^h$. We define the local finite-dimensional space and d.o.f. set as

$$\boldsymbol{\mathcal{V}}^{h,\mathfrak{E}} \coloneqq \{\boldsymbol{v}^h \in [\mathcal{H}^1(\mathfrak{E})]^2 \times \mathcal{H}^2(\mathfrak{E}) : v_\alpha^h|_{\partial\mathfrak{E}} \in C^0(\partial\mathfrak{E}), \boldsymbol{v}^h|_{\mathfrak{e}} \in [\mathbb{P}_1(\mathfrak{e})]^2 \times \mathbb{P}_3(\mathfrak{e}), v_{3,\nu}^h|_{\mathfrak{e}} \in \mathbb{P}_1(\mathfrak{e}), \forall \mathfrak{e} \subset \partial\mathfrak{E}\} \quad (13)$$

(of dimension $\dim(\boldsymbol{\mathcal{V}}^{h,\mathfrak{E}}) \equiv N^{\text{dof}} = 15$) and

$$\mathcal{D}^{\mathfrak{E}} \coloneqq \{\boldsymbol{v}^h(\mathfrak{v}_i), \nabla v_3^h(\mathfrak{v}_i)\}. \quad (14)$$

Only (boundary) d.o.f. on each element vertex $\mathfrak{v}_i$ are used, i.e. also that v_α^h and v_3^h are harmonic and bi-harmonic functions inside $\mathfrak{E}$, respectively. On each element edge $\mathfrak{e}_i$ we have $v_\alpha^h(\mathfrak{v}_i)$ and $v_\alpha^h(\mathfrak{v}_{i+1})$ to uniquely determine (up to) a linear polynomial, thus having $\mathcal{C}^0$-continuity of v_α^h. The same results for $v_{3,\nu}^h(\mathfrak{v}_i)$ and $v_{3,\nu}^h(\mathfrak{v}_{i+1})$. In addition, in order to have $\mathcal{C}^1$-continuity of v_3^h at the vertices, we use $v_3^h(\mathfrak{v}_i)$, $v_3^h(\mathfrak{v}_{i+1})$, $v_{3,\tau}^h(\mathfrak{v}_i)$ and $v_{3,\tau}^h(\mathfrak{v}_{i+1})$ to uniquely determine (up to) a cubic (Hermitian) polynomial. Noting that $\mathfrak{v}_4 = \mathfrak{v}_1$, let the interpolation on each edge be expressed by $\mathfrak{g} = \mathbf{H}\mathfrak{d}$, with $\mathfrak{g} = [\boldsymbol{v}^h(\mathfrak{e}_i) \quad v_{3,\nu}^h(\mathfrak{e}_i)]^T$,

$$\mathbf{H} = \begin{bmatrix} \varphi_{1,1} & 0 & 0 & 0 & 0 & \varphi_{1,2} & 0 & 0 & 0 & 0 \\ 0 & \varphi_{2,1} & 0 & 0 & 0 & 0 & \varphi_{2,2} & 0 & 0 & 0 \\ 0 & 0 & \varphi_{3,1} & \bar{\varphi}_{3,1} & 0 & 0 & 0 & \varphi_{3,2} & \bar{\varphi}_{3,2} & 0 \\ 0 & 0 & 0 & 0 & \varphi_{4,1} & 0 & 0 & 0 & 0 & \varphi_{4,2} \end{bmatrix}, \quad (15)$$

$\varphi_{j,\alpha}, j = 1, \ldots, 4$ the basis function of the edge j-th d.o.f. at the α-th edge node ($\varphi_{1,\alpha} = \varphi_{2,\alpha} = \varphi_{4,\alpha}$) and $\mathfrak{d} = [v_1^h(\mathfrak{v}_i) \quad v_2^h(\mathfrak{v}_i) \quad v_3^h(\mathfrak{v}_i) \quad v_{3,\tau}^h(\mathfrak{v}_i) \quad v_{3,\nu}^h(\mathfrak{v}_i) \quad v_1^h(\mathfrak{v}_{i+1}) \quad v_2^h(\mathfrak{v}_{i+1}) \quad v_3^h(\mathfrak{v}_{i+1}) \quad v_{3,\tau}^h(\mathfrak{v}_{i+1}) \quad v_{3,\nu}^h(\mathfrak{v}_{i+1})]^T$.

The global finite-dimensional space and d.o.f. set result

$$\boldsymbol{\mathcal{V}}^h = \{\boldsymbol{v}^h \in \boldsymbol{\mathcal{V}}_0 : \boldsymbol{v}^h|_{\mathfrak{E}} \in \boldsymbol{\mathcal{V}}^{h,\mathfrak{E}}, \forall \mathfrak{E} \subset \mathcal{T}^h\} \quad \text{and} \quad \mathcal{D} = \{\boldsymbol{v}^h(\mathfrak{v}), \nabla v_3^h(\mathfrak{v}), \forall \text{ internal vertex } \mathfrak{v}\}. \quad (16)$$

Let $\boldsymbol{v}^h = \Pi^{\mathfrak{E}} \boldsymbol{v}^h + (\mathrm{I} - \Pi^{\mathfrak{E}}) \boldsymbol{v}^h$, with I the identity map. The local projector operator $\Pi^{\mathfrak{E}} \equiv \Pi : \boldsymbol{\mathcal{V}}^{h,\mathfrak{E}} \to [\mathbb{P}_1(\mathfrak{E})]^2 \times \mathbb{P}_2(\mathfrak{E})$ is here defined such that, $\forall \boldsymbol{v}^h \in \boldsymbol{\mathcal{V}}^{h,\mathfrak{E}}$,

$$\begin{cases} \int_{\partial\mathfrak{E}} \Pi \boldsymbol{v}^h \, \mathrm{d}\tau = \int_{\partial\mathfrak{E}} \boldsymbol{v}^h \, \mathrm{d}\tau \\ \int_{\mathfrak{E}} \nabla \Pi^3 v_3^h \, \mathrm{d}\zeta = \int_{\mathfrak{E}} \nabla v_3^h \, \mathrm{d}\zeta \\ \tilde{a}^{\mathfrak{E}}(\boldsymbol{p}, \Pi \boldsymbol{v}^h - \boldsymbol{v}^h) = 0, \forall \boldsymbol{p} \in [\mathbb{P}_1(\mathfrak{E})]^2 \times \mathbb{P}_2(\mathfrak{E}) \end{cases}, \quad (17)$$

with $\Pi \boldsymbol{v}^h = \Pi^\alpha v_\alpha^h \boldsymbol{e}_\alpha^r + \Pi^3 v_3^h \boldsymbol{e}_3^r$ and $\tilde{a}^{\mathfrak{E}}(\bullet, \bullet) \coloneqq \int_{\mathfrak{E}} \boldsymbol{\varepsilon}_\alpha(\bullet) \cdot \boldsymbol{\varepsilon}_\alpha(\bullet) \, \mathrm{d}\zeta = \tilde{a}^{\mathfrak{E},\alpha}(\bullet, \bullet) + \tilde{a}^{\mathfrak{E},3}(\bullet, \bullet)$ (see e.g. eq. (10)). The first two and 3rd of eq. (17) relate to, respectively, the stability and consistency conditions the method requires. For now, let the projection be expressed by $\Pi \boldsymbol{v}^h = \boldsymbol{\Pi}\mathfrak{m}$, with

$$\boldsymbol{\Pi} = \begin{bmatrix} \pi_{11} & \pi_{12} & \pi_{13} & 0 & 0 & 0 \\ \pi_{21} & \pi_{22} & \pi_{23} & 0 & 0 & 0 \\ \pi_{31} & \pi_{32} & \pi_{33} & \pi_{34} & \pi_{35} & \pi_{36} \end{bmatrix} \quad \text{and} \quad \mathfrak{m} = \begin{bmatrix} 1 & \xi_1 & \xi_2 & \xi_1^2 & \xi_1\xi_2 & \xi_2^2 \end{bmatrix}^T. \quad (18)$$

In eq. (10) the terms $\nabla \cdot \mathbf{N}$ and $\nabla \cdot \mathbf{M}$ vanish by the chosen method order $(k^\alpha, k^3) = (1, 2)$. Then, by the 3rd condition of eq. (17),

$$\int_{\mathfrak{E}} \boldsymbol{\varepsilon}_\alpha(\boldsymbol{p}) \cdot \boldsymbol{\varepsilon}_\alpha(\Pi \boldsymbol{v}^h) \, \mathrm{d}\zeta = \int_{\mathfrak{E}} \boldsymbol{\varepsilon}_\alpha(\boldsymbol{p}) \cdot \boldsymbol{\varepsilon}_\alpha(\boldsymbol{v}^h) \, \mathrm{d}\zeta = \int_{\partial\mathfrak{E}} (\tilde{\mathbf{N}}(\boldsymbol{p}) : \boldsymbol{v}^h \otimes \boldsymbol{\nu} + \tilde{\mathbf{M}}(p_3) : \nabla v_3^h \otimes \boldsymbol{\nu}) \, \mathrm{d}\tau, \quad (19)$$

with $\tilde{\mathbf{N}} = \boldsymbol{\eta}_\alpha \otimes \boldsymbol{e}_\alpha^r$ and $\tilde{\mathbf{M}} = \boldsymbol{e}_3^r \times \boldsymbol{\kappa}_\alpha \otimes \boldsymbol{e}_\alpha^r$. Let a test function for eq. (19) be expressed by $\boldsymbol{p} = \mathbf{S}\mathfrak{m}$, with $\mathbf{S}$ as eq. $(18)_1$ but with arbitrary coefficients. The left-hand side of eq. (19) 1st equality may be exactly computed over the boundary by the divergence theorem (specialized to the plane), as it only has polynomials. The right-hand side of eq. (19) 2nd equality may be computed by the d.o.f. Then, part of $\boldsymbol{\Pi}$ is obtained by (with no summation convention)

$$\mathbf{G}_i \coloneqq \frac{\partial^2 \tilde{a}^{\mathfrak{E}}(\boldsymbol{p}, \Pi \boldsymbol{v}^h)}{\partial \boldsymbol{s}_i^a \partial \boldsymbol{\pi}_i^a}, \quad \boldsymbol{b}_i \coloneqq \frac{\partial \tilde{a}^{\mathfrak{E}}(\boldsymbol{p}, \boldsymbol{v}^h)}{\partial \boldsymbol{s}_i^a}, \quad \mathbf{G}_i \boldsymbol{\pi}_i^a = \boldsymbol{b}_i \quad \text{and} \quad \boldsymbol{\pi}_i^a = \mathbf{G}_i^{-1} \boldsymbol{b}_i, \tag{20}$$

with $\boldsymbol{\pi}_i^a \coloneqq [\pi_{iN_i^{\ker}+1} \quad \dots \quad \pi_{iN_i^k}]^T$, $\boldsymbol{s}_i^a \coloneqq [s_{iN_i^{\ker}+1} \quad \dots \quad s_{iN_i^k}]^T$, $N_\alpha^{\ker} \coloneqq \dim(\ker(a^{\mathfrak{E},\alpha})) = 1$, $N_3^{\ker} \coloneqq \dim(\ker(a^{\mathfrak{E},3})) = 3$, $N_\alpha^k \coloneqq \dim(\mathbb{P}_1(\mathfrak{E})) = 3$ and $N_3^k \coloneqq \dim(\mathbb{P}_2(\mathfrak{E})) = 6$. Now, to complete the projection definition we solve the equality of deflection gradients and mean displacements (from the remainder two conditions of eq. (17))

$$\int_{\mathfrak{E}} \nabla \Pi^3 v_3^h \, \mathrm{d}\zeta = \int_{\mathfrak{E}} \nabla v_3^h \, \mathrm{d}\zeta = \int_{\partial \mathfrak{E}} v_3^h \boldsymbol{\nu} \, \mathrm{d}\tau \quad \text{and} \quad \int_{\partial \mathfrak{E}} \Pi \boldsymbol{v}^h \, \mathrm{d}\tau = \int_{\partial \mathfrak{E}} \boldsymbol{v}^h \, \mathrm{d}\tau. \tag{21}$$

For the plane stress solution, let $\Pi \mathbf{E}_{33}$ be defined such that $\Pi \mathbf{T}_{33} = 0$. Then, from eq. (6),

$$\Pi \mathbf{E} = \frac{1}{2}(\Pi \mathbf{F} + \Pi \mathbf{F}^T - 2\mathbf{I}) + \Pi \mathbf{E}_{33} \boldsymbol{e}_3^r \otimes \boldsymbol{e}_3^r \quad \text{and} \quad \Pi \mathbf{T} = \lambda \mathrm{tr}(\Pi \mathbf{E}) \mathbf{I} + 2\mu \Pi \mathbf{E}. \tag{22}$$

The projected internal potential energy, constant in strains and curvatures, results

$$\Pi U^{\mathfrak{E}} = \frac{1}{2} a^{\mathfrak{E}}(\Pi \boldsymbol{u}^h, \Pi \boldsymbol{u}^h) = \frac{1}{2} \int_{\mathfrak{E}} \boldsymbol{\sigma}_\alpha(\Pi \boldsymbol{u}^h) \cdot \boldsymbol{\varepsilon}_\alpha(\Pi \boldsymbol{u}^h) \, \mathrm{d}\zeta. \tag{23}$$

Note that eq. (22) and so eq. (23) are computable once eq. (20) is solved.

The remainder is a stabilization term, say, $b^{\mathfrak{E}}(\bullet, \bullet)$ a bilinear form containing the orthogonal quantities w.r.t. $\Pi \boldsymbol{v}^h$ and $\nabla \Pi^3 v_3^h$, i.e. $\hat{\boldsymbol{v}}^h = (\mathrm{I} - \Pi)\boldsymbol{v}^h$ and $\nabla \hat{v}_3^h = \nabla(\mathrm{I} - \Pi^3) v_3^h$. It may be the sum of their inner products evaluated at the nodes and also conveniently scaled by, e.g. $\beta_\alpha = \frac{1}{2}\mathrm{tr}(\frac{\partial^2 \Pi U^{\mathfrak{E},\alpha}}{\partial \boldsymbol{d}^2})$ and $\beta_3 = \frac{1}{2}\frac{Eh^3}{12(1-\nu^2)}$ (flexural rigidity). The stabilization potential energy results

$$U_s^{\mathfrak{E}} = \frac{1}{2} b^{\mathfrak{E}}(\boldsymbol{u}^h, \boldsymbol{u}^h) \coloneqq \sum_{i=1}^{N^{\mathfrak{v}}} (\beta_\alpha \hat{u}_\alpha^h(\mathfrak{v}_i) \hat{u}_\alpha^h(\mathfrak{v}_i) + \beta_3 (|\mathfrak{E}|^{-1} \hat{u}_3^h(\mathfrak{v}_i) \hat{u}_3^h(\mathfrak{v}_i) + \nabla \hat{u}_3^h(\mathfrak{v}_i) \cdot \nabla \hat{u}_3^h(\mathfrak{v}_i))). \tag{24}$$

Note that all d.o.f. and conditions of eq. (17) (all components of $\boldsymbol{\Pi}$) are used in eq. (24). This in general is necessary for the stiffness matrix to have full rank. As shown in Wriggers et al. [5], another option for eq. (24) is to consider the edge errors, i.e.

$$U_s^{\mathfrak{E}} \coloneqq \sum_{i=1}^{N^{\mathfrak{e}}} \int_{\mathfrak{e}_i} (\beta_\alpha \hat{u}_\alpha^h(\mathfrak{e}_i) \hat{u}_\alpha^h(\mathfrak{e}_i) + \beta_3 (|\mathfrak{E}|^{-1} \hat{u}_3^h(\mathfrak{e}_i) \hat{u}_3^h(\mathfrak{e}_i) + \nabla \hat{u}_3^h(\mathfrak{e}_i) \cdot \nabla \hat{u}_3^h(\mathfrak{e}_i))) \, \mathrm{d}\tau. \tag{25}$$

Specializing eq. (11) with $\bar{\boldsymbol{m}} = \mathbf{0}$, the considered external potential energy is (see e.g. Mengolini et al. [4] and Brezzi and Marini [3])

$$U_{\text{ext}}^{h,\mathfrak{E}} = -\langle \bar{\boldsymbol{n}}^{h,g}, \boldsymbol{u}^{h,g} \rangle^{\mathfrak{E}} = -|\mathfrak{E}| \bar{\boldsymbol{n}}^{h,g} . \frac{1}{N^{\mathfrak{v}}} \sum_{i=1}^{N^{\mathfrak{v}}} \boldsymbol{u}^{h,g}(\mathfrak{v}_i). \tag{26}$$

Finally, with eq. (23), eq. (24) (or eq. (25)) and eq. (26), the total potential energy is

$$U^{h,\mathfrak{E}} = U_{\text{int}}^{h,\mathfrak{E}} + U_{\text{ext}}^{h,\mathfrak{E}} = \Pi U^{\mathfrak{E}} + U_s^{\mathfrak{E}} + U_{\text{ext}}^{h,\mathfrak{E}} = \frac{1}{2} a^{h,\mathfrak{E}}(\boldsymbol{u}^h, \boldsymbol{u}^h) - \langle \bar{\boldsymbol{n}}^{h,g}, \boldsymbol{u}^{h,g} \rangle^{\mathfrak{E}}. \tag{27}$$

Differentiation of eq. (27) w.r.t. $\boldsymbol{d}$ leads to the residual

$$\boldsymbol{r}^{h,\mathfrak{E}} = \frac{\partial U^{h,\mathfrak{E}}}{\partial \boldsymbol{d}}, \tag{28}$$

from which differentiation results in the stiffness matrix

$$\mathbf{K}^{h,\mathfrak{E}} = \frac{\partial \boldsymbol{r}^{h,\mathfrak{E}}}{\partial \boldsymbol{d}}, \tag{29}$$

both referred to the global system. Let they be assemble as $\boldsymbol{r}^h = \mathsf{A}_{\mathfrak{E} \in \mathcal{T}^h} \boldsymbol{r}^{h,\mathfrak{E}}$ and $\mathbf{K}^h = \mathsf{A}_{\mathfrak{E} \in \mathcal{T}^h} \mathbf{K}^{h,\mathfrak{E}}$. The discrete form of the theorem of potential energy or variational form, equivalent to the discrete counterpart of eq. (12), results

$$\begin{cases} \boldsymbol{u}^h \in \boldsymbol{\mathcal{V}}^h \\ \boldsymbol{r}^h = \mathbf{0} \end{cases}. \tag{30}$$

4 Results

We named the element using eq. (24) and eq. (25) as "VKLT3" and "VKLT3S2", respectively. The element and numerical results are implemented with the Wolfram Mathematica software system and the AceSystem, see e.g. Korelc and Wriggers [7]. Values are in SI units and current configurations are in true scale.

4.1 Partially clamped hyperbolic paraboloid shell

The 1st example data are a hyperbolic paraboloid Ω given by $z = x^2 - y^2$ and $-\frac{1}{2} \leq x, y \leq \frac{1}{2}$, thickness $h = 0.01$, $h = 0.001$ and $h = 0.0001$, partially clamped $\partial\Omega$, body load $f_3^b = -8 \times 10^3$, Young modulus $E = 2 \times 10^{11}$ and Poisson ratio $\nu = 0.3$. The analyzed solution is the vertical displacement at point "A", see Fig. 1 (left), and the global strain energy each for three span-to-thickness ratios $\frac{L}{h} = \frac{1}{h}$. Reference solutions are given by the extrapolation values in Tables 17 and 18 of Krysl and Chen [8].

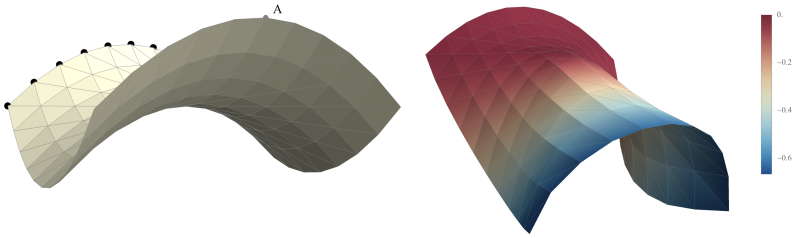

Figure 1. 1st example data, reference (left) and current (right) configurations ($N^{\mathfrak{E}} = 200$) ($\frac{L}{h} = 10000$).

Figure 2 shows convergence with mesh refinement and satisfactory relative error magnitudes using the element "VKLT3". This example shows the structure response to the action of the body load included in eq. (26). One sees better convergence for lesser thickness, which may be explained by the fact that the reference solutions come from a shear-flexible finite element. Nevertheless, for all $\frac{L}{h}$ the relative errors present asymptotically the same order of magnitude.

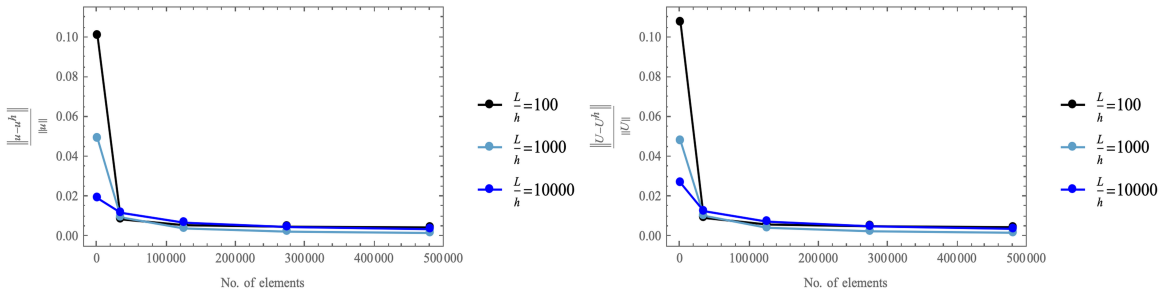

Figure 2. 1st example displacement (left) and strain energy (right) convergence curves.

4.2 Pinched hemispherical shell

The 2nd example data are a hemisphere Ω given by $x = 10\cos\theta\sin\phi$, $y = 10\cos\phi$, $z = 10\sin\theta\sin\phi$, $\theta \in [0, 2\pi)$ and $\phi \in [\frac{\pi}{10}, \frac{\pi}{2}]$, thickness $h = 0.04$, free $\partial\Omega$, concentrated loads of magnitude 100, Young modulus $E = 6.825 \times 10^7$ and Poisson ratio $\nu = 0.3$. The analyzed solutions are the vertical and lateral displacements at points "A" and "B", respectively, see Fig. 3 (left). For solution comparison we use the finite elements "T6-3iKL" of Sanchez et al. [9], "RMT3" and "RMT6", the last two being linear and quadratic triangular elements for Reissner-Mindlin shells (AceShare), respectively.

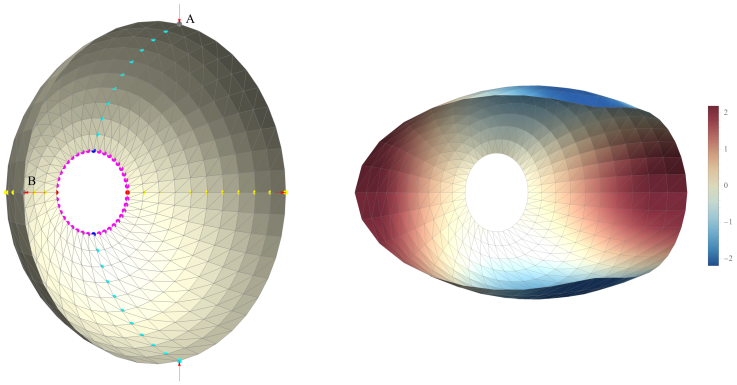

Figure 3. 2nd example data, reference (left) and current (right) configurations ($N^{\mathfrak{E}} = 800$).

Figure 4 shows convergence with mesh refinement and the efficiency of stabilization from eq. (24) and eq. (25), as no significant distinction between "VKLT3" and "VKLT3S2" is observed. In this example, they outperform the finite shell elements even having lesser N^{dof} compared to the lasts. Note that bending has an important role in this example. Also a triangle, the "T6-3iKL" presents quadratic displacement, nonconforming linear rotation and constant curvature approximation orders. "VKLT3", instead, has the same curvature approximation order from the projection (consistency), which is enhanced by the remainder (stability). Indeed, from eq. (13), eq. (14) and the discussion therein we have Hermitian out-of-plane displacements, which may explain part of the result.

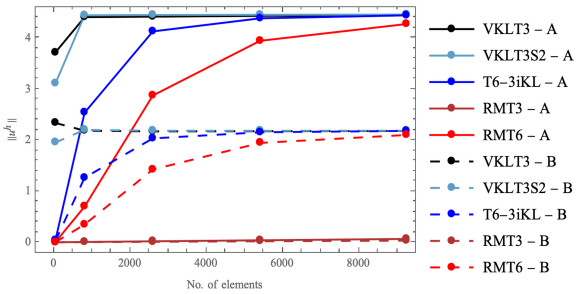

Figure 4. 2nd example convergence curves.

4.3 Thin Raasch hook

The 3rd example data are a two joined strips of circular arcs Ω with radius of magnitudes 0.3556 and 1.1684, cross section 0.000508×0.508, partially clamped $\partial\Omega$, shear load of magnitude 8.92898×10^{-7}, Young modulus $E = 2.32013 \times 10^{6}$ and Poisson ratio $\nu = 0.35$. The analyzed solution is the vertical displacement at point "A", see Fig. 5 (left). Solutions of the same elements used in the 2nd example and of the "VKLT3" extension to quadrilateral "VKLQ4" are compared.

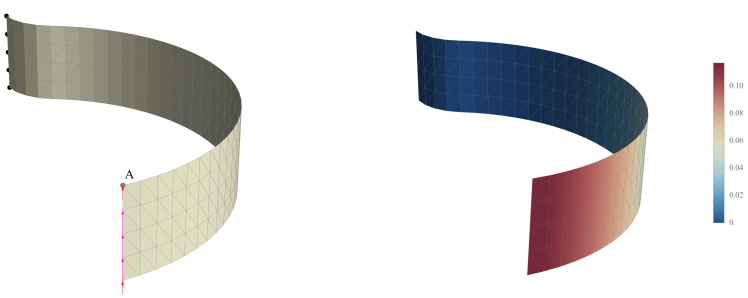

Figure 5. 3rd example data, reference (left) and current (right) configurations ($N^{\mathfrak{E}} = 288$).

Figure 6 shows convergence with mesh refinement using the proposed element. One sees that "VKLQ4" rapidly converges in this example. It presents more N^{dof} compared to "VKLT3" and "VKLT3S2". Fixing the mesh with similar total number of d.o.f. almost the same scenario results for coarse meshes, which shows the efficiency of the stabilization from eq. (24) as it has a more important role for a quadrilateral than for a triangle. On the other hand, "VKLQ4" application is restricted to cylindrical shells as aforementioned. The proposed triangular element outperforms "RMT3" and "RMT6", and presents similar convergence compared to "T6-3iKL".

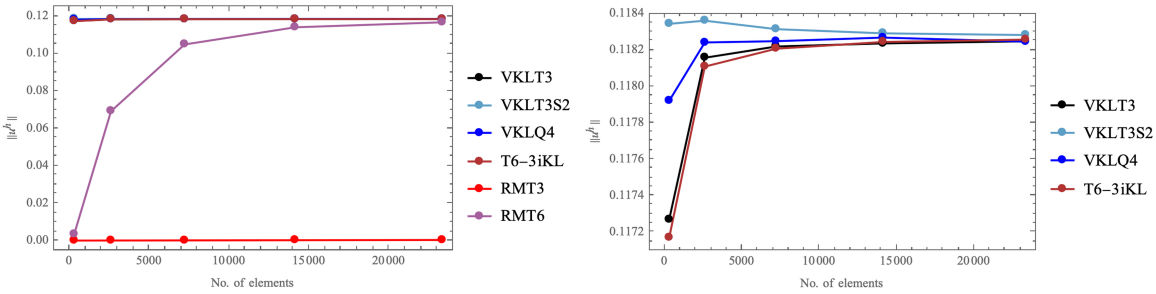

Figure 6. 3rd example convergence curves.

5 Conclusions

This work may show the VEM efficiency and versatility when applied in the context of structural theories. The 1st regards to the satisfactory accuracy reached in numerical results even for the present low-order case. The 2nd regards to, beyond the inherent aspects of the method (e.g. the various possible choices of element geometry, d.o.f., projection and stabilization schemes), the possibility of unifying aspects of different applications. Besides possible improvements of the present formulation regarding, e.g. projection and stabilization schemes, the vastness of possibilities for future works includes, e.g. element geometry, approximation order and nonlinear behavior generalizations.

Acknowledgements. This study was financed in part by the Coordenação de Aperfeiçoamento de Pessoal de Nível Superior – Brasil (CAPES) – Finance Code 001.

Authorship statement. The authors hereby confirm that they are the sole liable persons responsible for the authorship of this work and that all material that has been herein included as part of the present paper is either the property (and authorship) of the authors or has the permission of the owners to be included here.

References

[1] L. B. Da Veiga, F. Brezzi, A. Cangiani, G. Manzini, L. D. Marini, and A. Russo. Basic principles of virtual element methods. *Mathematical Models and Methods in Applied Sciences*, vol. 23, n. 01, pp. 199–214, 2013a.
[2] L. B. Da Veiga, F. Brezzi, and L. D. Marini. Virtual elements for linear elasticity problems. *SIAM Journal on Numerical Analysis*, vol. 51, n. 2, pp. 794–812, 2013b.
[3] F. Brezzi and L. D. Marini. Virtual element methods for plate bending problems. *Computer Methods in Applied Mechanics and Engineering*, vol. 253, pp. 455–462, 2013.
[4] M. Mengolini, M. F. Benedetto, and A. M. Aragón. An engineering perspective to the virtual element method and its interplay with the standard finite element method. *Computer Methods in Applied Mechanics and Engineering*, vol. 350, pp. 995–1023, 2019.
[5] P. Wriggers, B. Hudobivnik, and O. Allix. On two simple virtual Kirchhoff-Love plate elements for isotropic and anisotropic materials. *Computational Mechanics*, vol. 69, n. 2, pp. 615–637, 2022.
[6] P. M. Pimenta, E. S. Almeida Neto, and E. M. Campello. *A fully nonlinear thin shell model of Kirchhoff-Love type*. Springer, 2010.
[7] J. Korelc and P. Wriggers. *Automation of Finite Element Methods*. Springer, 2016.
[8] P. Krysl and J.-S. Chen. Benchmarking computational shell models. *Archives of Computational Methods in Engineering*, vol. 30, n. 1, pp. 301–315, 2023.
[9] M. L. Sanchez, P. M. Pimenta, and A. Ibrahimbegovic. A simple geometrically exact finite element for thin shells—part 1: statics. *Computational Mechanics*, pp. 1–21, 2023.